



E. K. LEE, N. H. CAIN, M. RAMADAN, J. D. LARKIN, C. WHITE, F. GRIFFIN, K. ROLL, T. NGUYEN, S. CALDEJON, S. CROSS, N. H. CAIN W. B. WAKEMAN, N. SJOQUIST, J. PERKINS, D. FENG, D. DENMAN, S. E. DEVRIES, C. SLAUGHTERBECK, D. SULLIVAN, D. WILLIAMS, D. MILLMAN, G. K. OCKER, P. LEDOCHOWITSCH, A. STEGER, R. VALENZA, K. MACE, S. WHITESIDE, E. LIANG, L. NG, C. FARRELL, M. A. BUICE, J. LECOQ

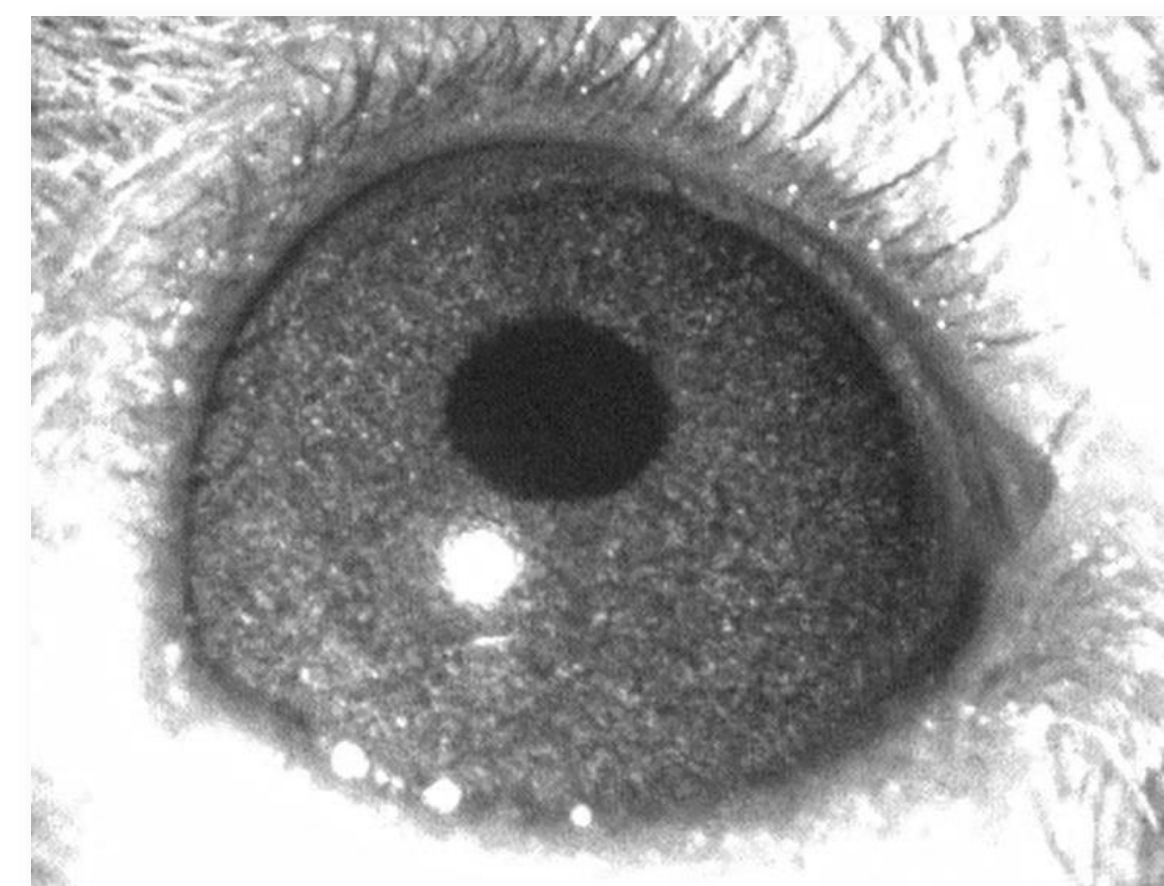
## Summary and Motivations

To give precise context to experiments investigating the visual cortex, it is necessary to delineate the particular sub-image of the stimulus incident on the retina – this is accomplished by the incorporation of eye position information. Here we present the eye tracking package **iTracker** which we combine with our hardware to create an integrated platform to collect eye tracking data across multiple modalities in a standardized and scalable manner. We further demonstrate the importance of eye tracking incorporation as pertains to receptive fields.

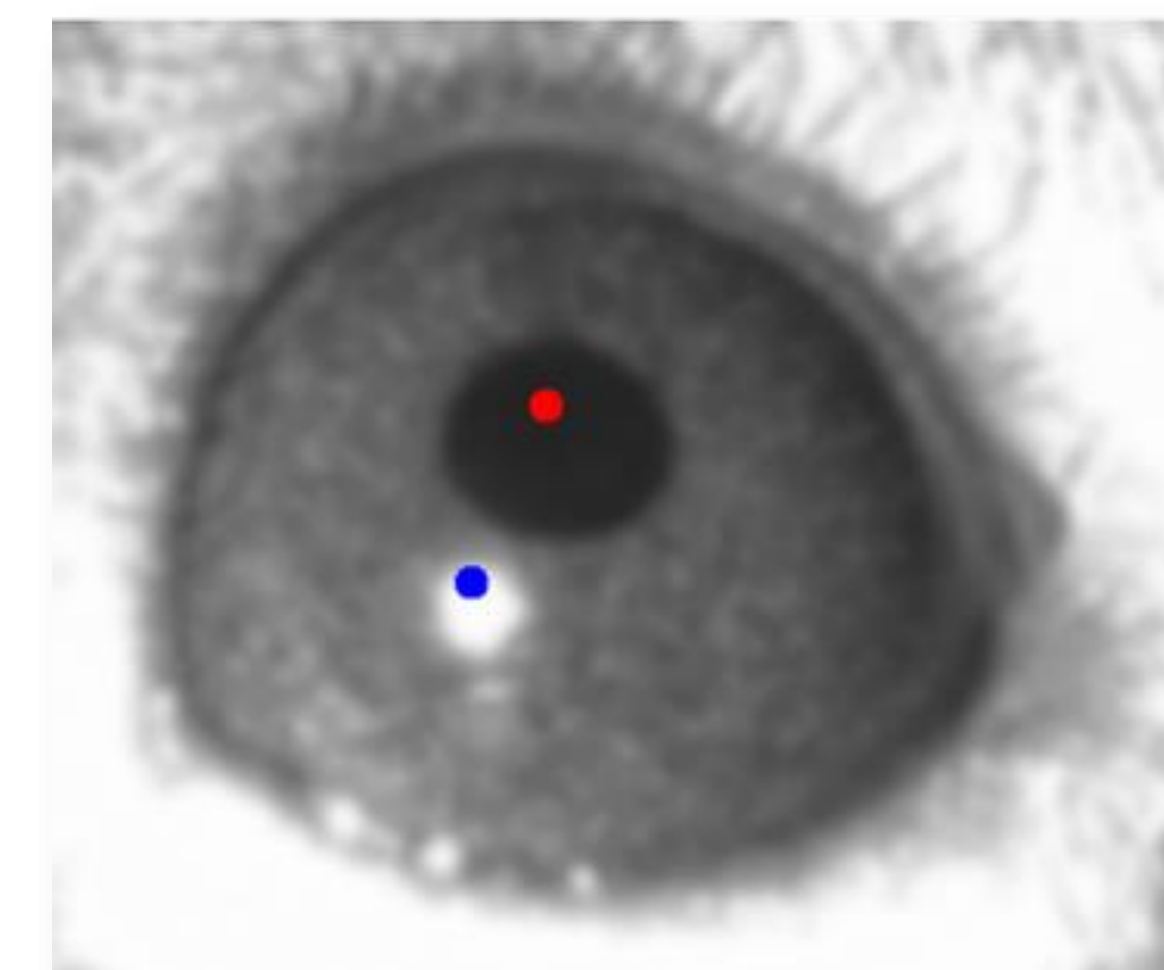
## iTracker Software and Starburst Algorithm

For our pipeline, we adapted the **Starburst Algorithm** originally described by Li D., Winfield D., Parkhurst D.J. (2005).

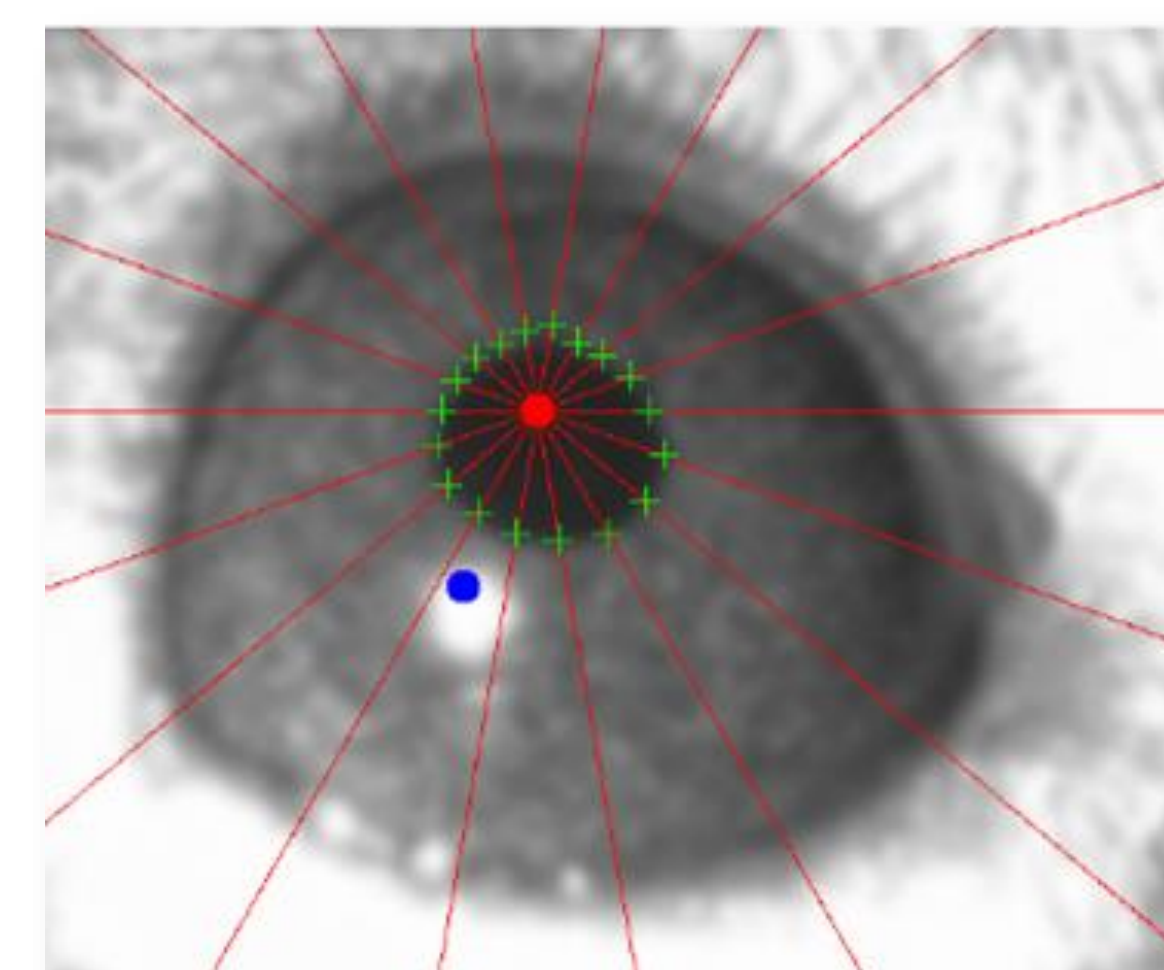
**Figure 1: A visual flowchart of the iTracker processing pipeline**



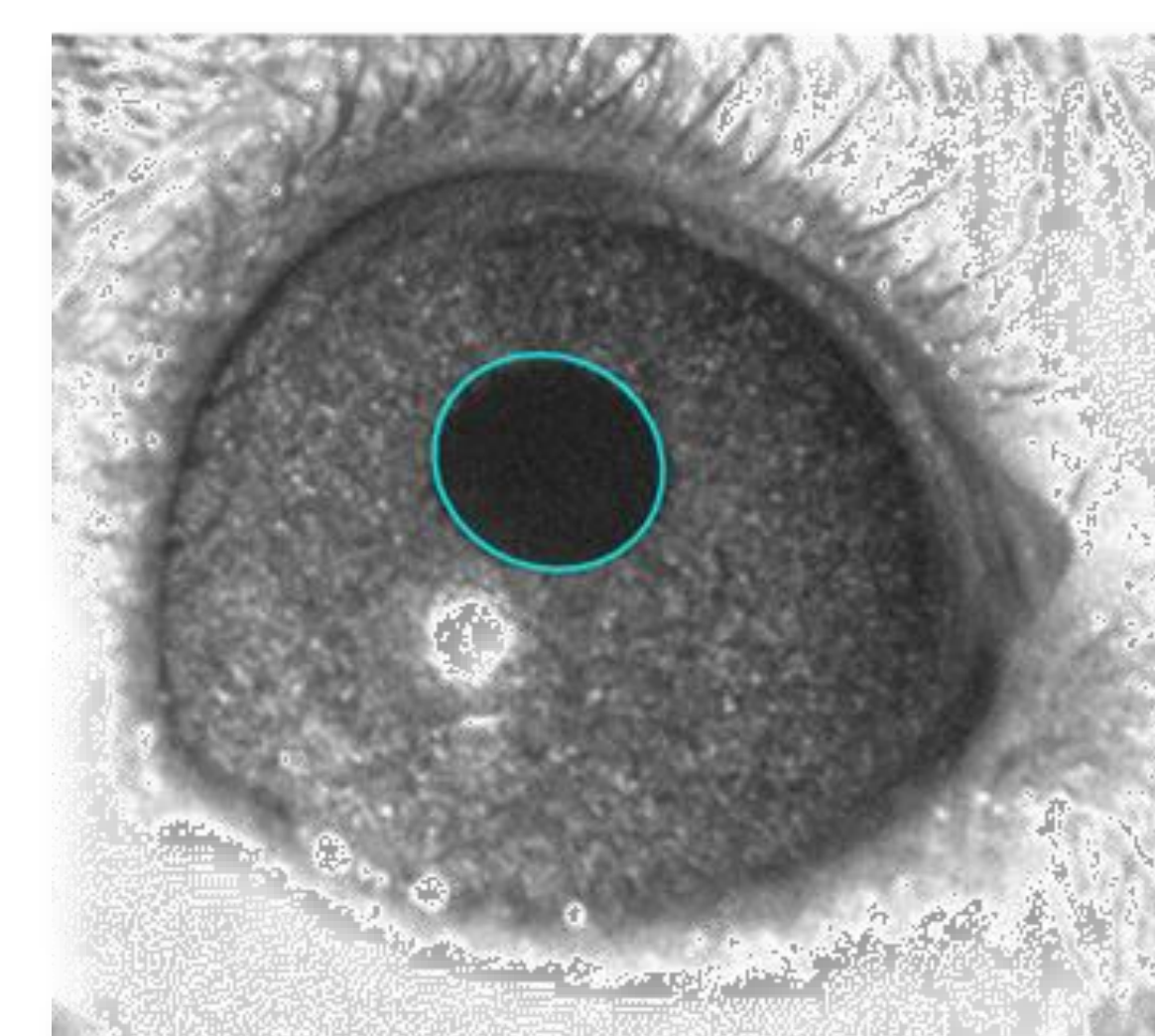
Images of the eye are obtained by the use of an IR-camera and IR-LED pointed at an IR-pass dichroic mirror that is coplanar with the mouse's eye. Each frame is extracted from the video and a bounding box is created around the eye and is used for all other frames.



The frame is then smoothed with a *median filter* and convolved with a black circle and white circle to find the pupil and corneal reflection (CR) respectively; the max convolution responses are the **seed points** for the *Starburst Algorithm* (red and blue dots for the pupil and CR respectively).

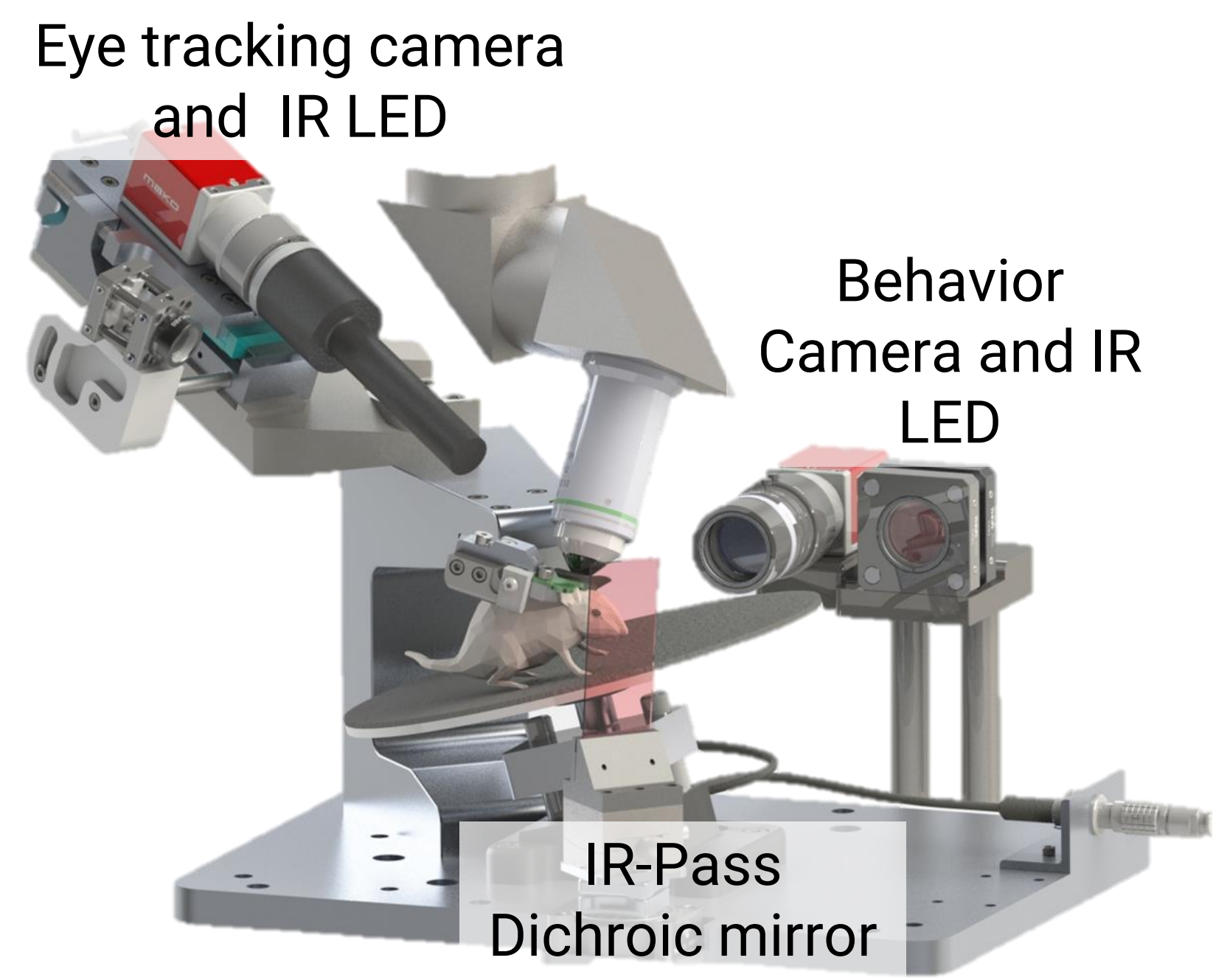


At each seed point, the Starburst Algorithm creates **rays**. Along each ray (from origin to radially outwards), a running average is calculated – when the pixel value exceeds some product of the running average pixel value  $\mu_{pix}$  and a user supplied a parameter  $\theta$ , a candidate point (small green cross) is marked (see equation below).

$$\tau = \theta * \mu_{pix}$$


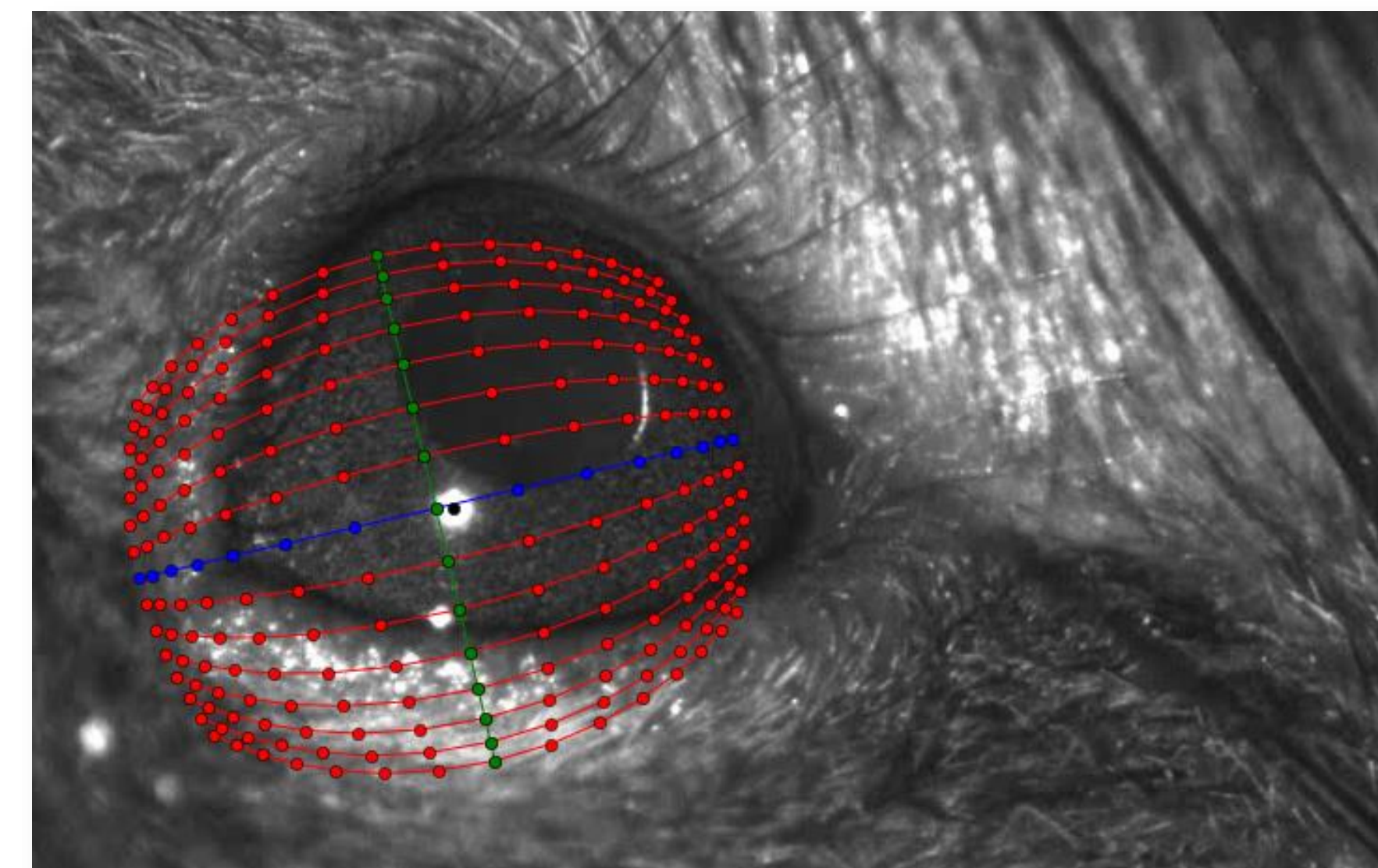
Candidate points are passed to a *random sample consensus* (RANSAC) which fits an ellipse. Using the ellipse parameters for both seed points, and knowing the geometry of our experimental rigs, we can determine pupil position and radius.

## 2-Photon Hardware Set-up



### Diagram of standardized eye tracking set-up on the 2-photon platform

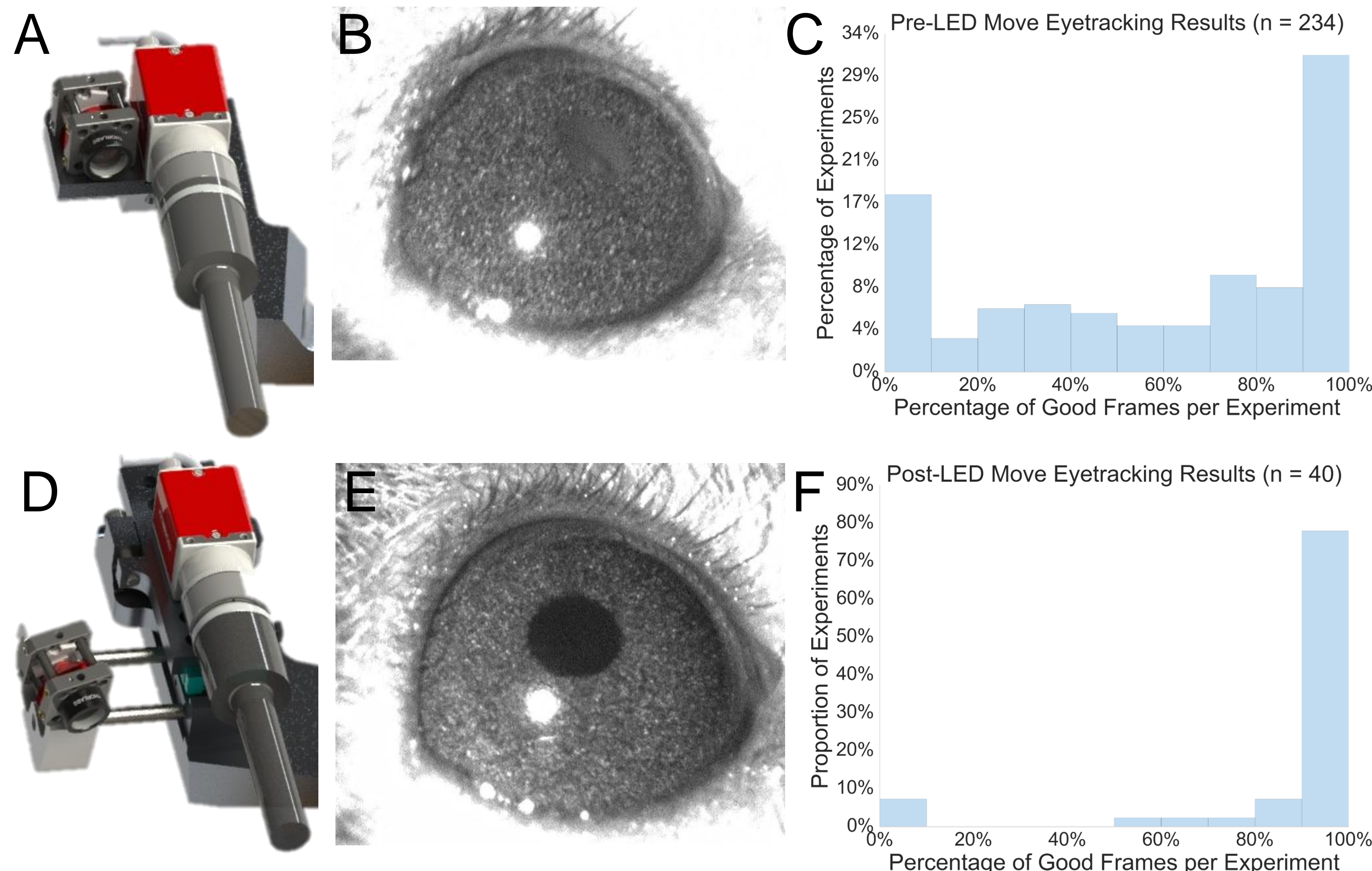
The eye tracking set-up has identical geometry across all five *in vivo* imaging rigs (and other modalities such as widefield and *in vivo* electrophysiology) of the Allen Brain Observatory pipeline enabling the collection of comparable data. It consists of an eye tracking IR-camera positioned 15° away from an IR-LED and directed at an IR-pass dichroic mirror. This mirror is positioned perpendicularly to the eye to allow for eye tracking while not impeding stimulus viewing.



### Mapping pupil position to the center of gaze on the stimulus screen

The eye position of the mouse is inferred by taking the center of the pupil ellipse and finding its projection (using the spherical mirror equation) from the spherical eye onto the flat screen assuming an eye diameter of 0.17 cm. From this calculation, a grid can be created which can be used to calculate the position of gaze from the pupil position. The LED corneal reflection is used as a fiducial mark to align the center and orientation of the grid given the known angular offset between the LED and camera. From this, the center of the pupil can be used to estimate the position of gaze.

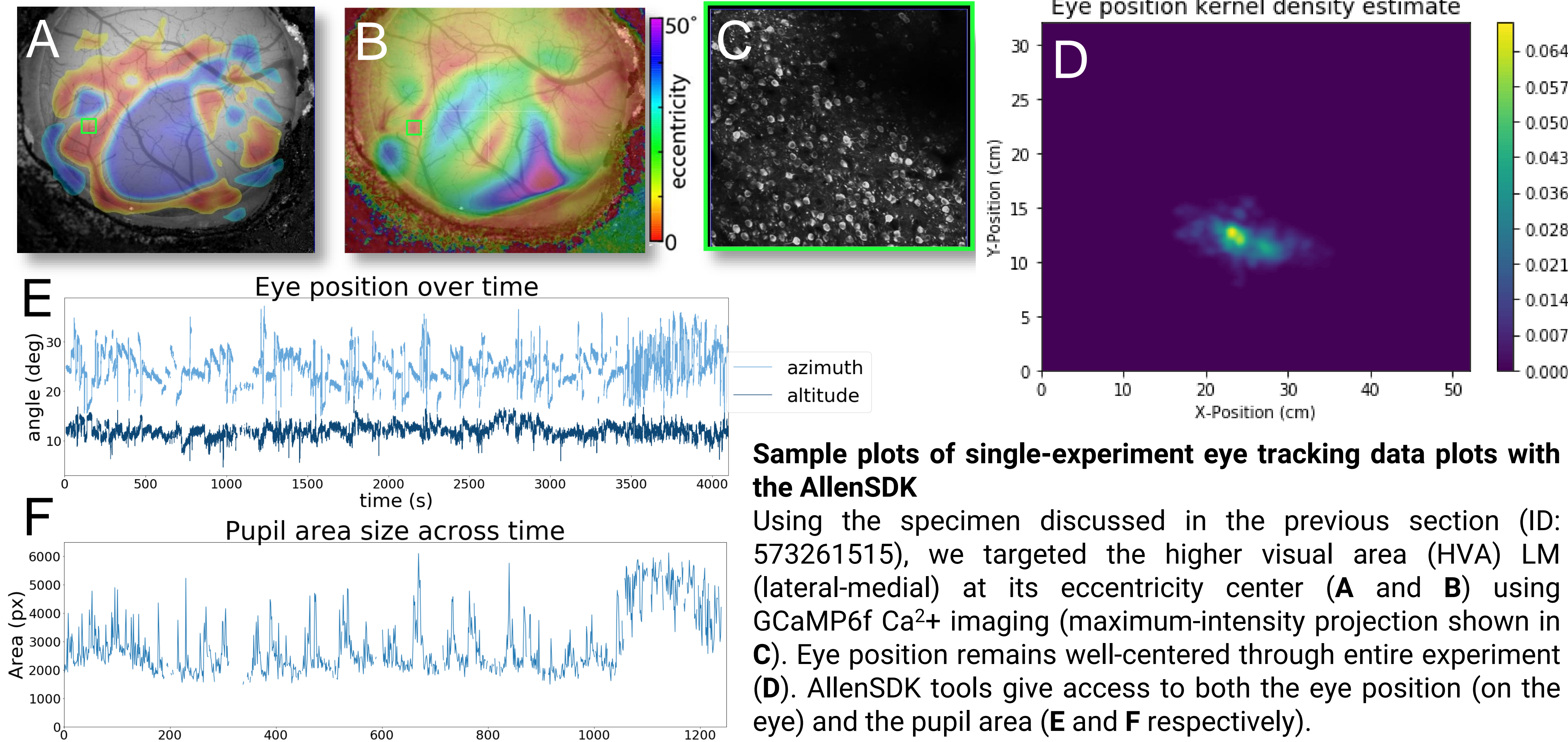
## Eye tracking performance before and after LED angular offset



Previous hardware implementations contained an LED to camera offset of **5.5° (A)** which resulted in failures in eye tracking due to the *bright pupil effect* (**B**) – the pupil color shifts from black to gray as incident light rays reflect into the camera at certain angles. This throws off the eye tracking algorithm which then detects spurious “pupil” candidates such as shadows or the eyelid. **At the 5.5° offset, only 76/234 (32%) experiments have greater than 95% of frames correctly annotated (C).**

Increasing the angular offset of the LED to the camera from 5.5° to 15° (**D**) almost completely eliminates the *bright pupil effect* and consistently elicits the *dark pupil effect* (**E**) and the pupil is consistently identified (**F**) – **at the 15° angular offset, 32/40 (80%) of experiments have greater than 95% of frames correctly annotated (H).**

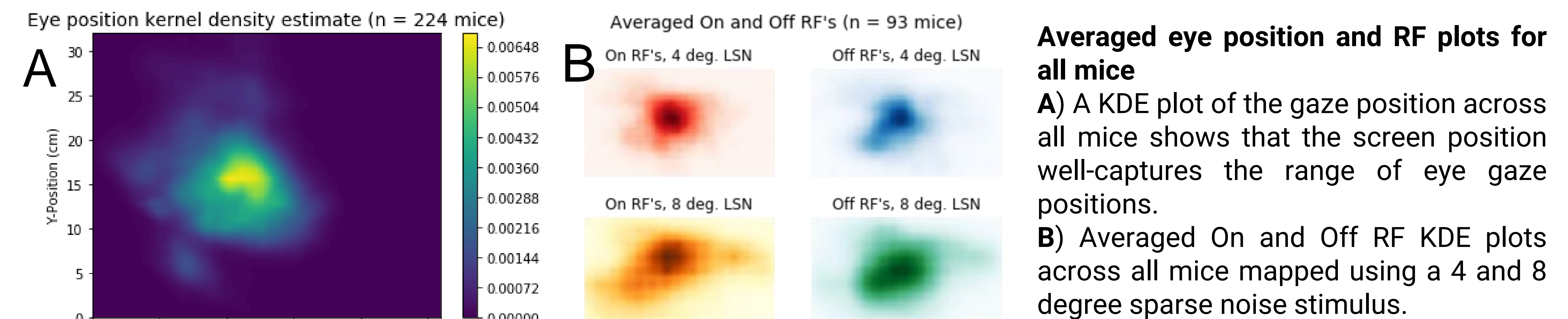
## Eye tracking and Data Output



### Sample plots of single-experiment eye tracking data plots with the AllenSDK

Using the specimen discussed in the previous section (ID: 573261515), we targeted the higher visual area (HVA) LM (lateral-medial) at its eccentricity center (**A** and **B**) using GCaMP6f Ca<sup>2+</sup> imaging (maximum-intensity projection shown in **C**). Eye position remains well-centered through entire experiment (**D**). AllenSDK tools give access to both the eye position (on the eye) and the pupil area (**E** and **F** respectively).

## Averaged eye tracking data

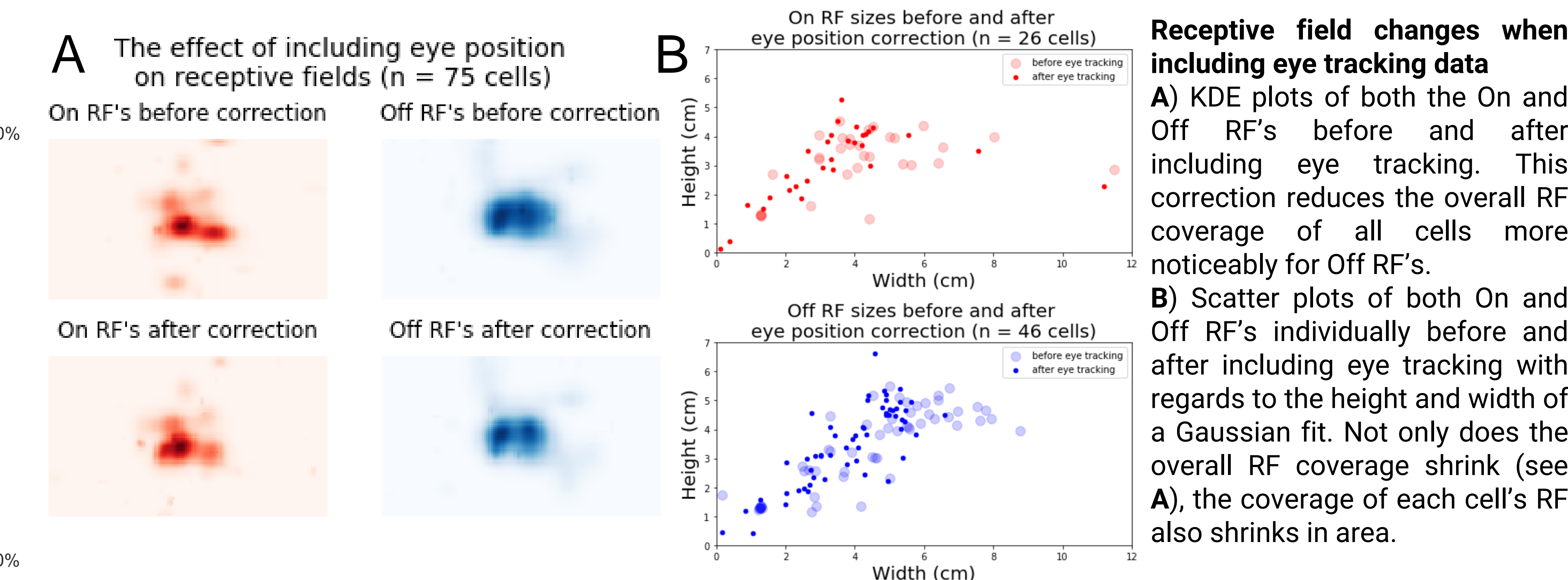


### Averaged eye position and RF plots for all mice

**A)** A KDE plot of the gaze position across all mice shows that the screen position well-captures the range of eye gaze positions.

**B)** Averaged On and Off RF KDE plots across all mice mapped using a 4 and 8 degree sparse noise stimulus.

## Receptive field changes before and after including eye tracking



### Receptive field changes when including eye tracking data

**A)** KDE plots of both the On and Off RF's before and after including eye tracking. This correction reduces the overall RF coverage of all cells more noticeably for Off RF's.

**B)** Scatter plots of both On and Off RF's individually before and after including eye tracking with regards to the height and width of a Gaussian fit. Not only does the overall RF coverage shrink (see **A**), the coverage of each cell's RF also shrinks in area.

## Conclusions/Discussions and Acknowledgments

With iTracker and our standardized cross-modality eye tracking setup, we are able to correct the eye position for all experiments in the pipeline for the Allen Brain Observatory. We have shown further how our algorithm works, that a significant angular offset is necessary for good eye tracking contrast conditions, examples of the data we can output, and the uses of such data in determining precise receptive fields which becomes important for stimuli such as static gratings with moderate to large spatial frequencies and any natural images or movies. The algorithm also allows for assessments of pupil diameter which is useful in the pupillometric assessment of animal engagement. Because of this tools potential utility in the neuroscientific community, we intend to release this tool in the near future. We wish to acknowledge all the work and countless hours put into this project by our teams whose names are too numerous to fit on a single poster. Most importantly, we also wish to thank Paul G. Allen and Jody Allen for their generosity, vision, and support.